AIAA-2004-3828

Propulsion Research Conducted at the Univ. of Maryland – Univ. of Michigan Space Vehicle Technology Institute

J. F. Driscoll[2],
C. C. Rasmussen[2],
M. Lewis[1], K. Yu[1],
W.J.A. Dahm[2],
A. Gupta[1],
A. Marshall[1]

[1]University of Maryland, College Park MD
[2]University of Michigan, Ann Arbor MI

40th AIAA/ASME/SAE/ASEE
Joint Propulsion Conference
Fort Lauderdale, Florida
11 - 14 July 2004

AIAA-2004-3828

Propulsion Research Conducted by the U. Maryland – U. Michigan Space Vehicle Technology Institute

J. F. Driscoll[2], C. C. Rasmussen[2], M. Lewis[1], K. Yu[1],
W.J.A. Dahm[2], A. Gupta[1], A. Marshall[1]

[1]University of Maryland, College Park MD
[2]University of Michigan, Ann Arbor MI

This paper consists of three parts: (a) a brief overview of NASA Project Constellation tasks associated with the throttlability, mixing and combustion instabilities in Liquid Rocket Engines, (b) a brief overview of air breathing propulsion activities associated with U.S. Air Force scramjet objectives, and (c) detailed research results associated with one specific topic – a new version of the classical Ozawa flame blowout curve that was determined for high speed propulsion devices. As part of the Space Vehicle Technology Institute (SVETI), the propulsion work is being conducted at the University of Maryland, the University of Michigan and at Johns Hopkins University.

Propulsion research has been conducted at the University of Maryland, the University of Michigan, and at Johns Hopkins University within a URETI center that has been supported by NASA and by the U.S. Air Force. Recent changes to the tasks have been made, so the first section of this paper describes the tasks that are associated with the Project Constellation effort that is supported by NASA. The second section describes the tasks that are funded by the U.S. Air Force in the area of air breathing propulsion for hypersonic vehicles.

A. Project Constellation tasks associated with Liquid Rocket Engines (NASA).

Within the Center the propulsion work is identified as Task 3 and the following areas have been identified.

3a. **System Analysis** - of a Baseline Liquid Rocket Engine
3b. **Improved Throttlability** - Experiments and Modeling
3c. **Heat Transfer, Mixing & Mixture Ratio Distribution** - high pressure experiments, and incorporation of our advanced Mixing Submodel into NASA's design codes
3d. **High-Speed Imaging Diagnostics** –applying our unique diagnostics to Liquid Rocket Combustion Chambers
3e. **Suppression of Combustion Instabilities –** using our unique experiments and our advanced CFD models of acoustics

3a. System Analysis - *of a Baseline Liquid Rocket Engine*

The Justification is to provide operating conditions for the experiments and the simulations being conducted by other members of the Center, a systems-level study will identify the operating parameters of a baseline Liquid Rocket Engine. This includes the baseline geometry, injector types, fuel and oxidizer flow rates, startup transients, throttlability range during lunar ascent and descent, unsteady operation, interactions between components , off-design operation. *The Objectives* are to identify conditions for the experiments and simulations in the other Tasks from systems-level study of a baseline Liquid Rocket Engine. *The Approach* is to perform design calculations collaboration with NASA. Some baseline parameters that will be provided for other groups in the Center are: chamber pressures, temperatures, fuel, oxidizer flowrates, injector types, chamber geometry, the acoustic frequencies, unsteady characteristics associated with startup and throttling.

3b. **Improved Throttlability** - *Experiments and Modeling*

The Justification for this task is that the local flow field near the injectors needs to be identified using advanced visualization diagnostics and computational modeling to understand flame standoff, heat transfer to walls, combustion instabilities, and startup and unsteady operation.
The Objectives are to develop an experimental database and scaling laws to characterize flame standoff, local recirculation, and local heat transfer to the injector wall. *The Approach* is to build and operate a small high-pressure single-injector experiments operated using hydrogen and oxygen at pressures to 60 atm. Flow visualization images will be obtained using laser diagnostics; results will be compared to those of a simultaneous modeling effort.

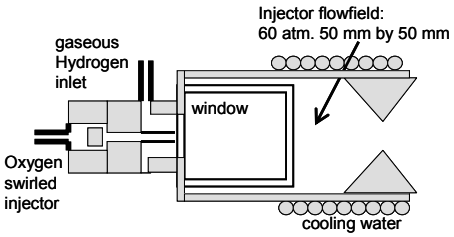

Figure A1. Planned Michigan Single-Element High-Pressure (60 atm) Injector Facility

The work will quantify flow field images as the device is throttled over the wide range associated with lunar descent and ascent. Images will quantify flame standoff and the distance required for fuel-oxidizer mixing. These two parameters are a good test of the predictive capabilities of the CFD models to be used.

3c. **Heat Transfer, Mixing & Mixture Ratio Distribution** - High Pressure Experiments, Improved Mixing Model

The Justification for this task is that current design models used by NASA need improved mixing submodels – which have been verified to be accurate over a range of high-pressure conditions, yet are not so detailed as to have impractical computation time. The new submodels need to account for supercritical fluid properties, high-pressure chemical kinetics, and high Reynolds numbers, which cause problems with current submodels. *The Objectives* are to develop improved and validated hybrid LES/RANS mixing submodels to add to existing NASA codes such as NCC, that include high-pressure properties yet are fast enough for practical design use. The *Approach* is to continue to obtain a benchmark mixing database at low and moderate pressures using our unique laser diagnostics, including Dual-Plane Stereo PIV, and to extend our fast LES/RANS mixing submodel to include high pressure phenomena. During the last two years a dramatically improved multifractal LES subgrid model has been developed and verified using advanced laser diagnostics. In the next year this new models will be extended to scalar mixing and mixing-chemistry coupling. Both multifractal RANS and LES subgrid models are being developed. To insure that the new subgrid model is realistic, another task is to obtain a unique database to assess and improve the model. Dual Plane Stereo PIV (DSPIV) diagnostics have been developed which allow, for the first time, accurate measurement of all components of the velocity gradients. The velocity gradients have been shown to be the key quantities that must be properly modeled to make RANS and multifractal LES subgrid mixing models realistic.

The unique Michigan Dual-Plane Stereo PIV DSPIV has been used to resolve and measure the small scale velocity gradients, including the vorticity fields, tensor strain rate fields, dissipation rate fields and enstrophy fields. This is the first-ever direct non-invasive measurement of this type to quantify turbulent mixing properties of high-Re shear flows. Results at jet Reynolds numbers of 6,000 and 30,000 were obtained recently and Re = 100,000 measurements currently are in progress. Measurements of velocity gradients in reacting flow also are in progress.

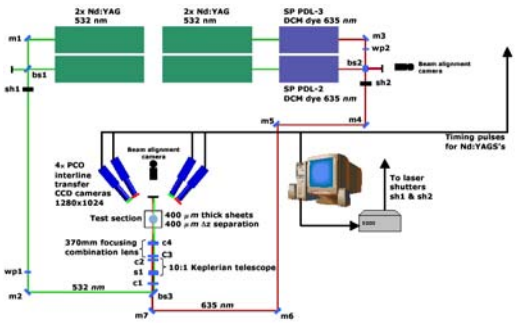

Figure A2. Schematic of the Michigan Dual Plane Stereo PIV (DSPIV) Diagnostics that Provide Fully-Resolved Velocity Gradients Necessary for LES and RANS Code Validation.

Figure A3. Photo of the Michigan Dual-Plane Stereo PIV Diagnostics

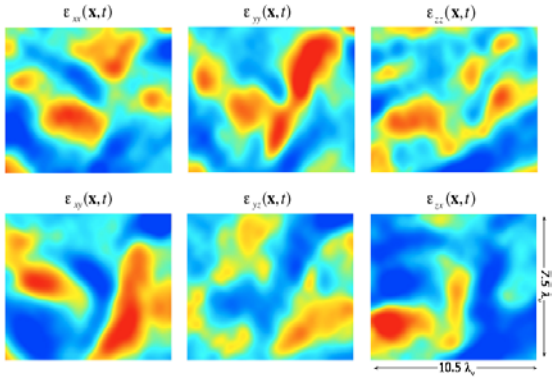

Figure A4. Images of the Measured Small-Scale Strain Rate Field. This information provides a sensitive test of RANS and LES mixing models and directly indicates the proper way to improve the submodels.

Film Cooling Research

As part of the Heat Transfer and Mixing task, film cooling experiments are being conducted at U. Maryland to eliminate the thermally induced mechanical stress induced by regenerative cooling. Research issues arise because film cooling can interact to affect the combustion. In the Maryland Film Cooling experiment near-wall mixing and heat transfer data have been obtained. Liquid hydrogen film cooling will be used in the future along with PIV and PLIF flow visualization diagnostics. The diagnostics are used to gain insight into the physical processes near hydrogen film-cooled surfaces and to determine scaling laws. The data will be used to validate heat transfer models in design codes for this complex type of cooling.

3d. **High-Speed Imaging Diagnostics** – for Liquid Rocket Combustion Chambers

The Justification for this task is that unsteady phenomena are potential "show stoppers" in Liquid Rocket Engines. Unsteady processes of interest are combustion instabilities, the transient startup, or unsteady throttling during lunar descent or ascent. Both the University of Michigan and the University of Maryland have and number of unique high-speed imaging diagnostics for this effort.

The objectives are to apply to the high pressure combustion rig in Fig. 1 certain unique High-Speed Imaging Diagnostics that we are now operating at several thousand frames per second.

Cinema Heat Release Imaging - OH chemiluminescence will be recorded at 10,000 frames/sec using our high speed Phantom 9.0 digital cameras. This identifies the flame standoff distance and the locations where mixing is sufficiently complete so that combustion can occur. During a throttling process, the local velocities change by orders of magnitude, and the unsteady movement of the reaction zones will be recorded.

Cinema PLIF – we have fluoresced tracer fluids at 2,000 images/sec to obtain a movie to see the time-history of the fuel location. For the high pressure work, we will add trace amounts of acetone added to the hydrogen fuel to obtain a high-speed movie of the fuel location, and compare the distance required to consume the fuel to the CFD simulation.

Cinema Schlieren - we have operational high speed Schlieren systems capable of obtaining movies showing the fuel and flame motions at 10,000 images/sec.

Cinema PIV – At low speed we have imaged the velocity field at 8,000 PIV images per second. We will investigate the feasibility of using our operational Cinema PIV diagnostics in the high pressure combustor, in order to visualize the unsteady motions of the recirculation zones.

F**ast-response diode laser** absorption spectroscopy is being set up to determine unsteady oscillations in fuel-oxidizer ratio and temperature. While these are line-of-sight measurements, the diagnostics are rugged and portable for use at NASA sites.

Piezoelectric Pressure Transducers – both Maryland and Michigan combustors will be fully

instrumented with fast pressure transducers and spectrum analyzers.

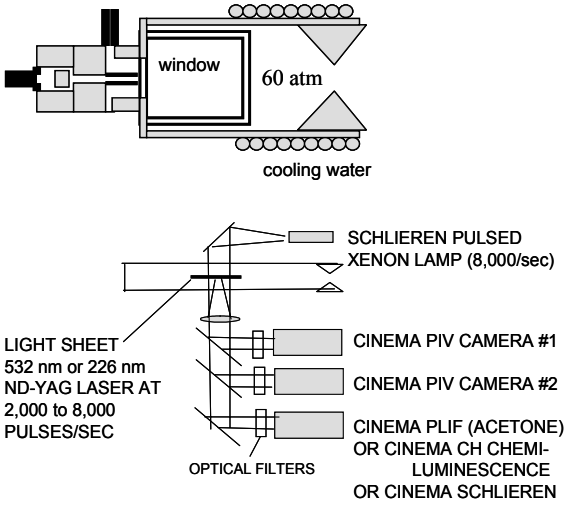

Figure A5. Schematic of the Operational Cinema PIV/PLIF System at the University of Michigan for use in the high pressure combustor.

Optical emission spectroscopy conducted at Maryland has provided instantaneous images of selected species of interest (mainly C2, CH and OH) using an ICCD camera. The time averaged spatial distribution of flame generated radicals (CH and OH) were processed using Abel Inversion technique wherein the initial 2-D projection is transformed into 3-D spatial distribution. Gas temperatures have been obtained from the ratio of intensities of two different C2 bands at wavelengths of 470 nm and 515 nm

3e. Suppression of Combustion Instabilities

The Justification for this task is that combustion instabilities are a potential "show stopper". An improved database and design models are needed that predict the correct trends, in order to reduce the number of trial-and-error experiments required to suppress combustion instabilities. Another goal is to explore passive control concepts. Improvements to NASA design codes to properly model the acoustic pressure field are needed. *The objective* are to develop passive control of spray combustion using Helmholtz cavities. Measurements to provide a well-characterized data base on combustion instabilities. Another objective is to develop an overall model of combustion instabilities (such as an n-tau time lag model) consisting of several components having validated transfer functions. The plan is to use the model to explore the high pressure regime that is not accessible in experiments. *The Approach* is to perform coordinated experiments and modeling for passive & active control of instabilities. Unsteady LES simulations can provide of transfer functions for each component in the overall model. The work will address Liquid Rocket Engine Instabilities due to several simultaneous sources: Propellant feed lines – interacting with the choked nozzle, the acoustics of the combustion chamber which cause a pressure/heat release correlation, and instabilities caused the vortices in the shear layers and recirculation zones.

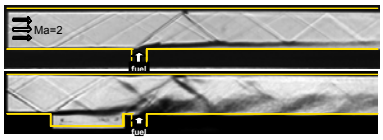

Add this cavity to provide resonance → Much thicker mixing layer observed

Figure A6. Previous Work at Maryland Showing How Cavities Can Be Used for Control of Mixing and Passive Control of Instabilities.

Maryland members of the SVETI team have many years of experience designing unique facilities to quantify cavity-flow interactions that affect instabilities. Figure 6 shows that by adding a cavity, the mixing layer can be increased in thickness by a factor of three.

The Maryland Facility for Active Control of Spray Combustion has been used to show how flow-induced instabilities interact with sprays that are undergoing combustion. Previous work has been conducted at low pressure with hydrocarbon fuels. Information gained will be applied to spray combustion – combustion instability interactions associated with high pressure liquid rocket engines.
Figure 7 shows the Maryland Facility for Active Control of Spray Combustion. PIV was used to obtain phase-resolved measurements of both the fuel droplet velocities and gas velocities. Both instantaneous and phase-lock averaged measurements were obtained. Comparison with non-reacting case revealed the effects of reaction and oscillations.

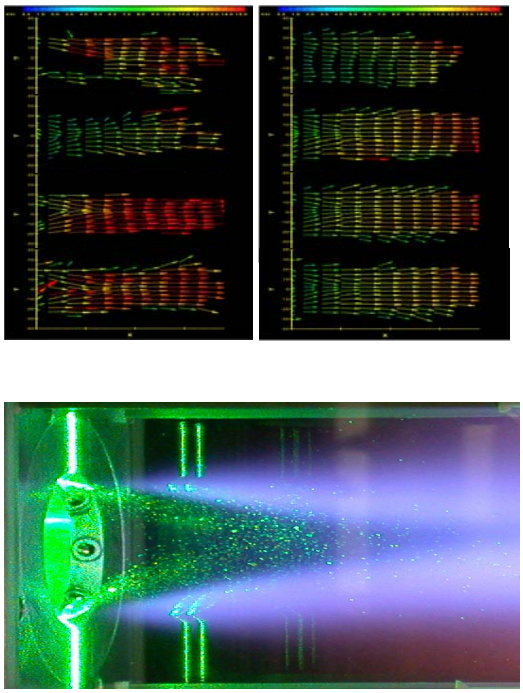

Fig. A7. The Maryland Facility for Active Control of Spray Combustion, Showing PIV Images of the Instantaneous and the Phase-Resolved Velocity Fields.

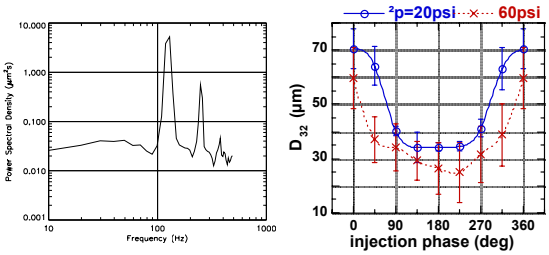

Figure A8. Results from the Maryland Facility for Active Control of Spray Combustion. The spray pattern is changed during rapid pulsing of the fuel injector, and the power spectra and droplet Sauter mean diameter were measured.

Figure 8 shows some results of applying active control of spray combustion. A rapidly pulsed liquid fuel injector was used. Controlled fuel sprays from practical actuators were characterized using phase-resolved planar Mie-scattering, PIV, fuel droplet sampling and analysis. The results showed that active control is caused by modulating the droplet size rather than the fuel mass flux.

B. Air-Breathing Propulsion Tasks for the U.S. Air Force – Technology to Support the Development of Hypersonic Vehicles

Ongoing work for the U.S. Air Force is continuing in order to meet the following objectives.

Task 3a. RBCC and TBCC Cycles
This is a systems-level study of propulsion cycles, including vehicle integration. Hybrid versus combined vs. parallel engines to be considered, building on experience of J58, ground-test RBCC's. The Objective is to map combined and hybrid cycles over the RLV Mach envelope, including mode transition. *The Approach* is to build a detailed set of engine decks for combined cycle engine concepts, with Pratt&Whitney - "hybrid" and true "combined" engines. A TBCC disk-actuator model has been used for compressor performance, identifying the Mach number limits and peak performance. The HySIDE vehicle design code was used.

3b. RBCC Modeling
Properties of Rocket-Based Combined Cycle engines must be identified and quantified, including geometry effects, engine dynamics, thermal choking and acoustic effects, unsteady loading, unstart, shock oscillations. To assist designers and develop design codes, scaling laws are needed to develop submodels of ejector efficiency, dissociation losses, and supersonic flameholding. Theobjective have been to study supersonic mixing and combustion between simulated rocket exhausts and supersonic air flow, and build detailed experimental database on supersonic combustion for model development, identify scaling laws which characterize flameholding, ejector efficiency, dissociation effects, combustion dynamics. The approach has been to build improved supersonic combustion facilities at U. Maryland and U.Michigan, to operate both supersonic combustors to measure: effect of temperature, pressure, cavity size on blowout limits, flame lengths. We have obtained high-resolution shadowgraph images of the shock wave and mixing layer above a cavity at Mach 2.5. The FLUENT CFD code was used to simulate of cavity-stabilized flames to identify limitations to current codes. We have interacted with Wright-Patterson AFB to conduct similar supersonic flameout and flow visualization imaging in the WPAFB facility.

3c. TBCC Modeling
Turbine-based engines will have unique issues associated with rotating machinery, seals, material temperature limits (including compressors). The objectives are to validate TBCC models for inclusion in vehicle studies; identify scaling issues, especially for thrust and weight. The approach has been to create a computer code to basic TBCC cycle decks for three configurations, integrate into full vehicle

One subtask addresses Turbine and Hot Section Survivability. The goal is to develop models for predicting heat load and component temperatures for integration with trajectory and vehicle studies and determination of operating range limitations. Cooling methods considered include: film cooling, Transpiration cooling, Effusion Cooling, and Thermal Barrier Coating.
The Maryland Film Cooling experiment was used to obtain heat transfer coefficients and set up IR surface temperature diagnostics and static and dynamic pressure instrumentation. The facility provides realistic wall conditions for combustion experiments.

3d. Mixing and Combustion - Improved Turbulence Model for High Speed Mixing

Accurate modeling of turbulent compressible mixing and supersonic combustion are critical to RLV design. Various injection schemes have been considered, but detailed physics, including diagnostics and control issues, remain unknown. Future RLV propulsion system development requires improved modeling tools; current turbulence models for mixing-chemistry coupling limit CFD accuracy. The objectives are to develop improved validated submodels for advanced computational propulsion codes, including RANS and multifractal LES subgrid models. A second goal is to extend models to scalar mixing and mixing-chemistry coupling. Dual Plane Stereo PIV diagnostics were developed and small scale velocity gradients were measured that are needed to improve RANS and multifractal LES subgrid models

Subtask: Supersonic Mixing Enhancement and Combustion Control
The objective of this subtask were to study supersonic mixing enhancement using natural acoustic resonance in wall cavity, assess benefits/penalty, and quantify the results
A novel mixing enhancement approach is being explored by combining passive control due to flow-induced cavity resonance with active excitation using a piezoelectric plate. Flow-induced cavity resonance generates large coherent structures in turbulent compressible mixing layer, thereby increasing the rate of fuel-air mixing. However, it was shown that mode hopping could occur under certain operating conditions potentially affecting the mixing benefit. Active forcing using a piezoelectric plate is being explored to provide a means to control the excitation frequency among many resonant frequencies.

(c) **Correlation of Blowout Limits of Cavity Strut, and Bluff-Body-Stabilized Non-premixed Flames in High-Speed Airflows**

This work identifies a scaling parameter (which is a modified Damkohler number) that is found to correlate the measured blowout limits of nonpremixed flames that are stabilized in high-speed air flows by wall-cavities, bluff-bodies and struts. Understanding the scaling of the combustor is needed to select the correct height of a cavity or step flameholder in a ramjet or a scramjet. This work focuses on nonpremixed conditions that occur when fuel is injected directly into a wall cavity or behind a strut, as is done with new designs. Thus the Damkohler number that is identified is different from of that of Zukowski and Ozawa, who considered the different case of premixed flames in afterburners. Nonpremixed conditions introduce a new parameter that is not relevant for premixed conditions: the location of the fuel injector with respect to the recirculation zone.

Approximately 140 measured values of blowout limits from eleven studies were found to collapse about a single curve (having rich and lean limit branches) if one uses the scaling parameter suggested by our analysis. The analysis is based on the idea that the propagation speed of the flame in the shear layer is matched to the velocity of the incoming gas. Hot products in the recirculation zone preheat the shear layer gases and increase the propagation speed of the flame. The analysis avoids an assumption that has been used previously – that the residence time of reactants in the recirculation zone is matched to some chemical reaction time. Experimental justification of the present approach is discussed.

This work addresses the issue of how to properly scale combustor properties in high-speed propulsion devices that use recirculation zones for flame stabilization. It is known that an

important nondimensional scaling parameter is the Damkohler number[1-5]. This number allows one to relate the required step height (H) in a laboratory device to that of a full-scale engine. For example, for the case of a premixed flame stabilized in an afterburner, Ozawa[2] has shown that the required step height H is given by:

$$\mathrm{Da} = \left(\frac{H}{U} / \frac{\alpha_0}{S_0^2}\right) \quad F = \exp\left[8.75\ (\phi - 1)^2\right] \qquad (1)$$

The quantity $(H/U)/(\alpha_0/S_0^2)$ F is defined as the critical Damkohler number (Da) at blowout for the premixed case. F is a scaling function that must be determined from premixed flame experiments. U is the freestream velocity, S_0 and α_0 are the stoichiometric laminar burning velocity and the thermal diffusivity at 300 K, 1 atm. Equation 1 states that that the Damkohler number is only a function of α; therefore blowout in a large scale device (i.e, for large values of H and U) will occur at the same Damkohler number in a small-scale device (for small values of H and U), if both devices have the same equivalence ratio ϕ.

Ozawa[2] determined the scaling function F in Eq. 1 for premixed flames by plotting measured values of H and ϕ. The blowout data for kerosene fuel collapsed to the single curve given by Eq. 1 for the following scaling function F:

$$F = \left[\frac{T_0}{300\,\mathrm{K}}\right]^{1.5} \left(\frac{p}{1\,\mathrm{atm}}\right) \left(\frac{d_e}{d}\right) \left(\frac{4760\ \mathrm{s}^{-1}}{S_0^2 / a_0}\right) \qquad (2)$$

T_0 and p are the stagnation temperature and pressure of the free stream and d_e/d is a factor that varies between 1 and 2 for circular and V-shaped flameholder geometries. One can see from Eqs. 1 and 2 that a smaller step height is necessary if one increases T_0, S_0 or p, or if one reduces U, or if the value of ϕ approaches unity. Ozawa noted that the hydrocarbon fuel data showed reasonable agreement with Eq.1, but the hydrogen fuel data did not, for reasons that are still not known.

Figure 1 is a plot of Eq. 1, which is named the Ozawa curve and is used to estimate the blowout limits of subsonic, premixed hydrocarbon-air flames in afterburners. Note that the horizontal axis is logarithmic, so the function on the right side of Eq. 1 describes the parabola shown in Fig. 1.

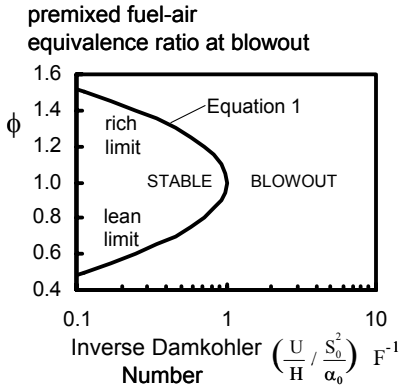

Figure 1. Plot of the Ozawa Curve[2] (Eq. 1) Which Correlates Blowout Limits of Premixed Subsonic Flames.

Unfortunately, Eqs. 1 and 2 and Fig. 1 apply only to premixed flames because they assume that the combustion always occurs at the known equivalence ratio (ϕ) of the premixed reactants. For nonpremixed flames, no similar correlation of flame blowout limits has been reported in the literature. Different parameters and different concepts are needed because the local equivalence ratio where combustion occurs is not known a priori. There is a need for such information; in new ramjet and scramjet designs, nonpremixed conditions are employed to avoid the flashback, combustion instabilities, and engine unstart associated with premixing the reactants far upstream of the combustor. New flameholder concepts include wall cavities[6-12], struts[13,14], rear-facing steps, bluff-bodies[15-20], a "trapped vortex"[21,22] and other ideas[23-25]. These geometries can provide good flame stability with low pressure losses, and the walls can be effectively cooled. In most cases the fuel is injected just upstream or directly into a recirculation zone, and there are large spatial variations in the fuel-air ratio. For example, sometimes a cavity recirculation zone can become filled with pure fuel. Therefore the goals of the present work are to:

(a) use concepts that apply to nonpremixed flames to derive a scaling relation analogous to Eq. 1 in which the Damkohler number appears;
(b) identify a scaling function (G) which is analogous to the scaling function F given by Eq. 2 for premixed flames;

(c) plot measured blowout limits from eleven nonpremixed flame studies to determine if the scaling function G does tend to collapse the data to the single curve that is suggested by the analysis; the geometries considered were rear-facing steps, cavities and struts;
(d) use the analysis to identify sensitive parameters that need to be better quantified to improve the prediction of blowout limits.

Figure 2 shows the three different types of flameholders considered: a step, a wall cavity, and a strut. They have three basic components: a shear layer, a recirculation zone, and an outer free stream of air. Figure 3 illustrates the locations where fuel is normally injected. In some cases the fuel is injected upstream of the step at location (a) so the fuel enters directly into the shear layer. However, for other cases the fuel is injected directly into the recirculation zone at location (d). The injector location becomes an important new variable that does not appear in previous analyses[3-4] of premixed flame blowout limits. For example, it has been observed[9, 21] that if fuel is injected directly into the RZ at location (d), it is easier to "flood" the cavity with a fuel-rich mixture, forcing the flammable region to move upward and into the high-speed airstream. This tends to suppress the fuel-rich blowout limit (i.e., it limits the amount of fuel that can be injected before the flame blows out). If fuel is injected upstream of the step at location (a), then much of the fuel may bypass the cavity. This tends to enhance the fuel-rich limit but it suppresses the lean limit. If fuel is injected at location (b) it also enters directly into the recirculation zone. Fuel that is injected at location (c) is observed[9] to flow upward into the shear layer, as shown in Fig. 3.

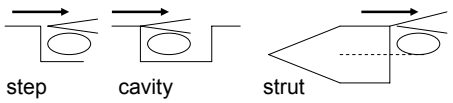

Figure 2. Schematic Showing That Step,Cavity and Strut Flameholders Consist of the Same Components: a Shear Layer Located Between the Free Stream and the Recirculation Zone.

Figure 4 provides a physical explanation of the fuel-rich blowout limit. The rich limit is defined as the condition for which an excessive mass flowrate of fuel is injected, causing the flame to blowout and disappear. The solid line within the shear layer in Fig. 4a represents the stoichiometric contour. Experiments[27-29] have confirmed that a lifted nonpremixed flame is located along the stoichiometric contour. The curve labeled "$U_s(x)$" in Fig. 4b represents the gas velocity along that contour. The horizontal lines labeled S_{base} represent the propagation speed of the flame base. This propagation speed depends on the unburned gas temperature just upstream of the flame base, which is elevated because of heat transfer from the hot gases in the recirculation zone. The x-location where the curve of gas

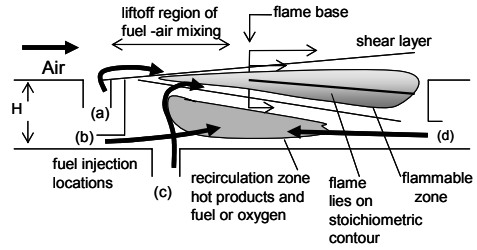

Figure 3. Components of the Shear Layer in the Nonpremixed Flames Considered. A flammable zone exists between the air stream and the recirculation zone. Bluff-body flames typically have the fuel injector at location (b), while strut fuel injectors are type (a) or (b), and cavity-injectors are of type (a), (c) or (d).

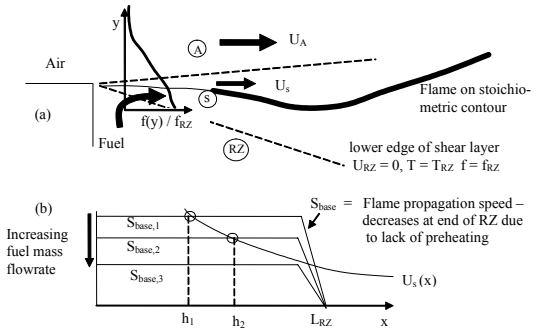

Figure 4. A Physical Explanation of the Rich Blowout Limit. (a)Recirculating products increase the temperature at lower edge of shear layer (T_{RZ}). (b) increasing the fuel flowrate mixes cold fuel into the RZ, reduces T_{RZ} and the flame propagation speed S_{base} until it is less than the oncoming gas velocity.

velocity U_s crosses over the curve of propagation speed S_{base} in Fig. 4b is the liftoff height h_1. As the fuel flowrate is increased toward the rich limit, more cold fuel enters the recirculation zone, so the fuel and products in the RZ become cooler, so the gas temperature upstream of the flame base decreases. This causes the curves of propagation speed (S_{base}) to decrease as shown. The liftoff distance (h) shown in Fig. 4b increases until it exceeds L_{RZ} and the reactants are no longer preheated, so rich blowout occurs. In addition, the stoichiometric contour is forced to move upwards into the higher velocity free stream, which is destabilizing.

Correlation of Blowout Limits for Nonpremixed Flames

In order to quantify the blowout limits, it is useful to define the overall fuel-air equivalence ratio of a nonpremixed flame (ϕ_O). It is not implied that this overall equivalence ratio is an indicator of any local equivalence ratio. Instead ϕ_O simply is defined such that when ϕ_O sufficiently exceeds 1 there is too much fuel injected which causes a "rich limit" blowout. When ϕ_O is sufficiently less than one, not enough fuel is injected so a "lean limit" blowout occurs. To define ϕ_O it is necessary to first define a characteristic air mass flowrate. The total mass flow rate of air contained in the free stream is not appropriate, since this flowrate can be made arbitrarily large by increasing the height of the freestream above the recirculation zone, and this height is not a relevant parameter. Winterfeld[6] and Kundu et al.[4] present data showing that the air mass flow rate entrained into a recirculation zone is proportional to $\rho_A\ U_A\ H\ W$. Therefore, following the convention set by Winterfeld[7], the characteristic air mass flowrate is defined as:

$$m_A = 0.01\ \rho_A\ U_A\ H\ W \qquad (3)$$

Thus m_A is one percent of the free stream air flowrate that would flow through an area equal to the product of the step height H and width W. In this definition the value of one percent is chosen for convenience; it happens to cause the rich and lean limits to converge at an overall equivalence ratio of approximately unity, as shown below. This definition of air mass flowrate can be justified because it is proportional to the mass flowrate of air that is entrained into the shear layer over the streamwise distance from x = 0 to x = L_{RZ}. Consider one side of a shear layer where the layer boundary is at a height δ_A above the layer centerline. The air mass flowrate crossing this boundary must be $\rho_A U_A \delta_A W$. Furthermore, δ_A is proportional to L_{RZ}, which is proportional to the step height H, since the constant L_{RZ}/H is assumed to be known. It is noted that m_A is used only for scaling purposes; it is not assumed that all of this air entrained is available for combustor or that it enters the recirculation zone. For an axisymmetric bluff-body, the step height H is defined as the radius of the bluff-body, and the width W is defined as the bluff-body circumference.

The overall equivalence ratio is defined as:

$$\phi_O = \frac{m_F}{m_A}\, r_S^{-1} \qquad (4)$$

where m_F is the total mass flowrate of fuel injected and m_A is the characteristic air mass flowrate given by Eq. 3. The quantity r_s is the stoichiometric fuel-air ratio which has the value listed in Table 1 for several fuels. Note that for nonpremixed flames, the combustion chemistry does not occur at the overall equivalence ratio ϕ_O; instead the flame tends to locate itself near the local stochiometric contour, as confirmed by experiments[27-29]. Varying ϕ_O only has an indirect effect on the chemistry; it can move the location of the stoichiometric contour farther from the hot recirculation zone, which lowers the temperatures of the gas entering the flame.

The Damhohler number is defined in a manner analogous to that of Ozawa[2]:

$$Da_{LEAN} = \left(\frac{H}{U_A} / \frac{\alpha_0}{S_0^2}\right)_{LEAN}\ G_{LEAN} \qquad (5)$$

$$Da_{RICH} = \left(\frac{H}{U_A} / \frac{\alpha_0}{S_0^2}\right)_{RICH}\ G_{RICH} \qquad (6)$$

where G is a scaling function for nonpremixed flames that is described below .

The following empirical approach was used. The analysis of the next section provides equations for the scaling functions G_{RICH} and G_{LEAN}. These equations contain four empirical constants. If the empirical constants are chosen correctly, the analysis indicates that flame

blowout measurements should collapse to the two curves:

$$Da_{LEAN}^{-1} = \phi_O \quad (7)$$

$$Da_{RICH}^{-1} = \phi_O^{-1} \quad (8)$$

To assess this idea, approximately 140 values of flame blowout limits were tabulated from the results of eleven nonpremixed flame studies. Then each of the four empirical constants was set to an optimum value to determine if the proposed scaling function G does indeed collapse the nonpremixed flame data to the curves represented by Eqs. 7 and 8.

Figure 5 shows the results of the effort to correlate rich and lean blowout limits from eleven nonpremixed flame studies. The vertical axis represents the overall equivalence ratio defined by Eqs. 3 and 4 and the horizontal axis represents the inverse of the Damkohler number. Values plotted in Fig. 5 includes measurements reported for supersonic bluff-body stabilizers and hydrogen fuel by Winterfeld[7] (Fig.14), Yoon et al.[15] (Fig. 7) and Huh et al.[16] (Fig. 3). Supersonic cavity-stabilized flame blowout limits were measured by Rasmussen et al.[9] (Figs. 2,9,10) and Gruber et al.[10] (Fig. 11), who used ethylene fuel. Supersonic struts and hydrogen fuel were used by Niioka et al.[13] (Figs. 3, 4). Also shown in Fig. 5 are results for the subsonic bluff-body hydrocarbon flames of Schefer et al.[17], Chen et al.[18], Masri and Bilger[19], the subsonic cavity-stabilized flame of Hsu and Roquemore[21], and the subsonic swirl flames of Feikema et al.[23,24]. The lean and rich blowout limits are defined to occur when the fuel mass flowrate is either decreased or increased sufficiently to cause flame blowout. Some values of these limits are tabulated in the Appendix, along with other properties such as the fuel and air temperatures, free stream velocities and step heights.

To plot the data in Fig. 5, the scaling function G was chosen to be the function that is suggested by the analysis of the next section, which is:

$$G_{LEAN} = \left[A \frac{(T_{AD} - T_{0A})}{300\,K} \frac{f_s}{2} + \frac{T_{0A}}{300\,K}\right]^2 \left(\frac{p}{1\,atm}\right)^{0.8} r_s \left(\frac{W}{H}\right) \beta_4$$

$$G_{RICH} = \left[\left[B \frac{(T_{AD} - T_F)}{300\,K} + \frac{(T_F - T_{0A})}{300\,K}\right] C + \frac{T_{0A}}{300\,K}\right]^2 \left(\frac{p}{1\,atm}\right)^{0.8} D$$

where: $A = [1 + \beta_3 (L_{RZ}/H)\, r_s^{-1}\, \phi_O^{-1}]^{-1}$ (11a)

$$B = [1 + \beta_1 (H / L_{RZ})\, r_s\, \phi_O]^{-1} \quad (11b)$$

$$C = f_s [1 - B]^{-1} \quad D = (L_{RZ} / H)\, (1-C)^{-1}\, \phi_O\, \beta_2 \quad (11c)$$

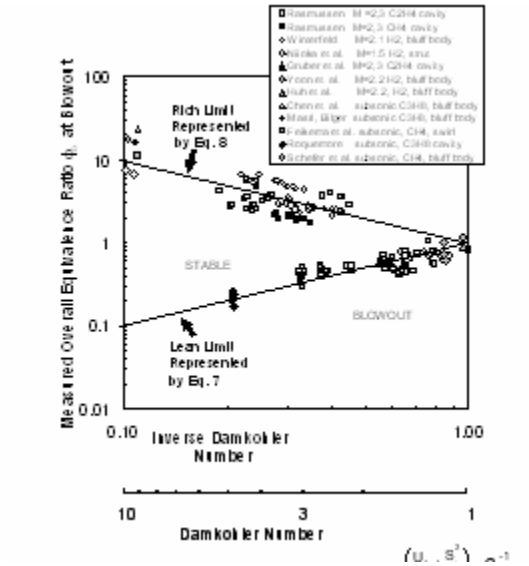

Figure 5. Correlation of Measured Rich and Lean Blowout Limits from Eleven Nonpremixed FlameStudies Compared to Eqs. 7 and 8 (Solid Lines), Using the Proposed Scaling Parameter G.

T_{AD} is the adiabatic flame temperature listed in Table 1, T_F is the fuel injection temperature and T_{0A} is the air stagnation temperature. The ratio L_{RZ}/H is a known constant that is approximately 2 for a bluff body. For a wall cavity it equals the cavity length to height ratio. Values of the stoichiometric mixture fraction (f_s) are listed in Table 1. There are four empirical constants (β_1, β_2, β_3, and β_4) in Eqs. 9-11 and the values of these constants that were chosen to best collapse the data are listed in Table 2. β_1 is shown below to be proportional to the fraction of fuel entrained into the shear layer, so the value of β_1 is larger when the fuel is injected directly into the shear layer from locations A and C that are identified in Fig. 3. β_3 is proportional to the fraction of fuel entrained into the recirculation zone, so the value of β_3 is larger when fuel is injected directly into the recirculation zone from locations B and D.

It can be concluded from Fig. 5 that most the measurements are clustered about the two solid lines, which represent Eqs. 7 and 8. The upper (rich limit) curve has a slope of -1, and the lower (lean limit) curve has a slope of +1. Therefore the empirical constants listed in Table 1, along with the selected scaling function G, adequately correlate the measurements. The standard deviation in the scatter in the data

points, divided by the mean value, is 45% for the lean limit and 65% for the rich limit, for an average uncertainty of 55%. This scatter is primarily caused by two factors. First, it is predicted by Eqs. 5 and 6 and by previous researchers[2-5] that if the type of fuel is changed, the step height required will scale as S_0^{-2} so that the step height must be 36 times larger if the hydrogen fuel is replaced with methane. While methane flames are less stable than hydrogen flames, this predicted factor of 36 is larger than that which is measured. Notice that the open squares in Fig. 5, which correspond to ethylene fuel, lie above those obtained using methane fuel (solid squares) for otherwise identical conditions[9]. Above these lie the hydrogen data points (open circles). This indicates that the S_0^2 scaling predicted by Eq. 6 is only approximately correct.

A second source of scatter in Fig. 5 is the assumption that the complex entrainment of hot products and fuel into the recirculation zone can be correlated using the four empirical constants β_1-β_4. Factors not considered include the molecular weight of the fuel and details about the fuel injection process. However, the purpose of this paper is not to provide an accurate model of all aspects of the complex flameholding process; the goal is to develop empirical relations that are useful to engine designers. Additional research is needed to better quantify the entrainment of hot products into recirculation zones.

	M	Fuel	H mm	Da	T_{0A} K	U_A m/s	m_F g/s	m_A g/s	ϕ_O	G	Limit
Winterfeld[7]	2.1	H_2	10	3.30	375	530	0.40	4.00	3.45	0.53	rich
Bluff Body	2.1	H_2	10	1.13	375	610	0.09	4.60	0.69	0.21	lean
Rasmussen[9]	2.0	C_2H_4	17	3.33	590	711	1.98	9.16	3.18	1.85	rich
Wall Cavity	2.0	C_2H_4	17	1.26	590	711	0.34	9.16	0.56	0.71	lean
Niioka[13] Strut	1.5	H_2	6	16.6	500	546	0.56	1.80	10.7	2.40	rich
Gruber[10] Cavity	2.0	C_2H_4	17	1.54	590	711	0.33	8.60	0.56	0.71	lean
Schefer[29]	0.3	CH_4	25	9.60	296	105	5.10	5.00	17.6	3.30	rich
Masri & Bilger[19]	0.1	C_3H_8	30	9.10	296	35	2.40	1.00	15.6	1.22	rich
Hsu, Roquemore[21]	0.1	C_3H_8	30	4.83	296	42	0.06	3.90	0.24	0.55	lean

Table 3. Values of the Step Height (H) and Damkohler Number (Da) for Various Flame Blowout Limits That Are Plotted in Figure 5.

Figure 6 provides additional evidence that the proposed scaling function G is realistic. Blowout limits were calculated using Eqs. 5-11 for two air stagnation temperatures: 600 K and 1000 K. The fuel is hydrogen and the fuel injection temperatures are equal to the air stagnation temperatures. Note that no scaling factor G appears on the horizontal axis, so the two curves do not collapse. The calculated rich and lean blowout limits merge at a value of ϕ_O of approximately unity, and the higher temperature conditions shift the curves to the right, leading to a larger range of stable conditions. Previously, Yoon et al.[15] reported blowout measurements for conditions similar to those of Fig. 6. The measured set of curves of Yoon et al. look similar to those in Fig. 6.

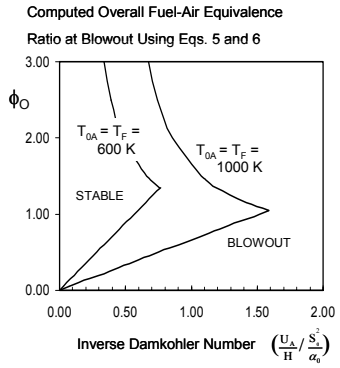

Figure 6. A Plot of Eqs. 4 and 5 Showing That the Stable Regime Becomes Larger as the Stagnation Temperature of the Air is Increased. These curves are similar to the measurements [15]. Fuel = H2. $L_{RZ}/H = 2.0$, $W/H = 6$.

Effect of Fuel Injection Location, Mach No.

Inspection of the data reported by Rasmussen et al.[9] indicates some differences between fuel injection at the cavity floor location (C in Fig. 4) and at location (D), which is on the downstream wall of the cavity. Injecting fuel from floor location C forces fuel to go directly upward into the shear layer, so much of the fuel will be transported over the cavity and will not enter the downstream region of the recirculation zone. Therefore large fuel flowrates injected at C will not flood the cavity with fuel. However, large fuel flowrates injected at location D will go directly into the recirculation zone and will flood the cavity with fuel. Consistent with this idea, the rich blowout limits of Ref. 9 are observed to be larger for injection at location C than at D.

To account for these observations, the constant β_3 (in Eq. 11c) should be smaller when fuel is injected at C than at D, since the analysis below indicates that β_3 is proportional to the fraction of fuel that is entrained into the recirculation zone, rather than into the shear layer. Therefore β_3 was chosen to be 0.002 for injection location C and 0.004 for location D.

These values provide the best fit to the data to Eqs. 7 an 8.

The Mach number was varied over a wide range (from 0.2 to 3) in the experiments used to generate the data in Fig. 5. The Mach number was not included in the scaling factor G, yet this scaling factor was found to adequately collapse the data to cluster about the two straight lines in Fig. 5. Therefore it is concluded that blowout is primarily affected by the air velocity U_A which appears in the Damkohler number (Eqs. 5 and 6), and that additional effects of compressibility due to Mach number variations were not observed.

Comparison of Nonpremixed and Premixed Flame Blowout Limits

It is observed that the curve in Fig. 5 that correlates nonpremixed flame blowout limits has the same general appearance as the Ozawa curve (Fig. 1) for premixed flames. In both figures the measurements collapse to a curve which reaches a maximum value of Da^{-1} at an equivalence ratio of approximately one. Another similarity is that both of the scaling functions F and G increase as one increases the stagnation temperature or the static pressure of the freestream, as indicated by Eqs. 2, 9 and 10. This is expected, since a larger value of F or G indicates that the flame becomes more stable.This work identifies several major differences between the nonpremixed and premixed blowout limits. First, the scaling functions F (Eq. 2) and G (Eqs. 9, 10) have a different form. The location where the fuel is injected is important in the nonpremixed case (and it affects the parameters β_2 and β_3 in Eq. 11 and Table 2), but there is no local fuel injection in the premixed case. The stoichiometric mixture fraction (f_s) plays an important role in the nonpremixed case (in Eq. 9) but it does not appear in the premixed scaling function (Eq. 2). For example, a nonpremixed hydrogen-air flame must lie close to the high-velocity air stream since stoichiometry requires that the fuel and air mix such that the mixture is 99.1% air and 2.9% fuel by mass (f_s =0.029). The location of a premixed flame depends on a different parameter - its turbulent burning velocity. Another difference is that the temperatures of the fuel and air appear as separate terms in Eqs. 9 and 10, since they can be injected with different temperatures in the nonpremixed case, but not in a premixed situation. The definition of equivalence ratio also differs; for the premixed case ϕ is proportional to the actual amount of fuel that is locally mixed with air, so ϕ controls the local chemistry. For the nonpremixed case ϕ_O simply indicates the mass flow of fuel relative to that of air; the chemistry is not required to occur at a local equivalence ratio equal to ϕ_O. It is concluded that the Ozawa curve (Eq.1) cannot accurately be applied to nonpremixed flames; instead the proposed new scaling function G yields an adequate correlation of blowout limits.

Derivation of the Scaling Function G_{RICH} for the Rich Limit

In this section a formula for the scaling function G is derived using shear-layer similarity concepts. A number of simplifying assumptions have to be made, including the following.

1) Upstream of a lifted flame base there exists a flammable zone between the fuel-rich and fuel-lean regions, and a stoichiometric contour exists. Experimental evidence that the flammable zone exists is provided by Refs. 27-29.
2) The fundamental assumption for flame stability[30] is that even though the fuel and air initially are nonpremixed, they mix in the liftoff region so the flame base is a premixed flame that propagates at a velocity (S_{base}) that is equal to the gas velocity along the stoichiometric contour (U_s), thus:

$$S_{base}(T_s) = U_s \qquad (12)$$

The location "s" is marked in Fig. 4a; U_s is the gas velocity at that location. S_{base} is a function of the temperature (T_s) of the reactants just upstream of the flame base, and the reactants are heated by heat transfer from the recirculation zone. Experimental verification of Eq. 12 is provided by Upatnieks, et al.[31] and Muniz and Mungal[32]. Another requirement for stability is that:

$$d(S_{base})/dx > d(U_s)dx. \qquad (13)$$

This requirement ensures that if the flame is perturbed to move downstream, at the new location the propagation speed will exceed the local gas velocity, so the flame will propagate back to its original location.

3) Rich blowout is observed in experiments[9] to occur when the fuel mass flowrate is increased sufficiently to force the flame liftoff distance (h) to move downstream and exceed the length of the recirculation zone:

$$h = L_{RZ} \qquad \text{rich blowout} \qquad (14)$$

The gas upstream of the flame base is heated by heat transfer from the recirculation zone, and this no longer occurs when h exceeds L_{RZ}. Lean blowout will be considered in the next section.

4) It is assumed that the flame base always is located within the shear layer and not within the recirculation zone. There is experimental evidence to justify this assumption. The stoichiometric fuel-air ratio for hydrocarbon and hydrogen fuels does not exceed 0.07, thus the stoichiometric contour is forced to be much closer to the air stream (where the local fuel-air ratio is zero) than to any fuel-rich region, where the fuel-air ratio is infinite. Measurements by Winterfeld[6,7] and by Kalt et al.[33] indicate that the recirculation zone is filled with either hot products and fuel (near the rich blowout limit), or hot product and air (near the lean limit), but it never contains a mixture of fuel and air. Kalt et al.[33] (Fig, 5a) show that measured mixture fraction always is above the stoichiometric value in the recirculation zone of a bluff-body flame, indicating that only fuel and products exist there; their Raman measurements also show that the flammable zone (where significant oxygen exists) is only in the shear layer that exists between the recirculation zone and the air free stream.
5) It is assumed that blowout is not governed by the requirement that the fluid residence time in the recirculation zone is matched to some chemical reaction time, which has been assumed in the past[3] for premixed flames. This idea assumes that a "distributed reaction zone" exists instead of a "flame". Instead, images of Ratner et al. [34] confirm that flames exist and not "distributed reaction zones" for the nonpremixed conditions considered here. They report images of very thin CH layers (that are less than 1 mm thick) within the shear layer (between a recirculation zone and air), and see no evidence of distributed reactions.
6) In the liftoff region of the shear layer (upstream of any chemical reaction) it is assumed that there is similarity between the profiles of mixture fraction (f), stagnation temperature T_0, and gas velocity U:

$$\frac{f(y)}{f_{RZ}} = \frac{T_0(y) - T_{0A}}{T_{RZ} - T_{0A}} = \frac{U_A - U(y)}{U_A - U_{RZ}} \qquad (15)$$

This relation is similar to one that is valid in jet flows; it follows from the similarity between the equations representing the conservation of mixture fraction, energy and momentum where the axial pressure gradients are small. A typical profile of $f(y)/f_{RZ}$ is shown in Fig. 4. All three of the quantities equated in Eq. 15 have a value of zero on the upper side of the shear layer, and have a value of one on the lower side.

Some justification for the above assumptions is provided by Fig. 7. Rasmussen et al. photographed the chemiluminescense from a cavity stabilized Mach 2.0 ethylene-air supersonic flame. As the fuel flowrate is increased near the rich limit, Figs. 7a and 7b show that the flame base move downstream. Near the lean limit, as the fuel flowrate is decreased, the flame base moves upstream.

Based on the above six assumptions, the problem reduces to that of a flame that is stabilized in a stratified premixed shear layer. The boundary conditions on the air side are uniform and known ($U= U_A$, $T_0 = T_{0A}$, $f = 0$). On the lower side of the shear layer, the boundary conditions are complicated. We choose to define the lower edge of the shear layer as the location where the axial velocity is zero. Thus the lower part of the shear layer overlaps the upper portion of the recirculation zone. At this lower edge, $T=T_{RZ}$ and $f = f_{RZ}$. In the recirculation zone it is assumed that there is a uniform temperature and a uniform mixture of either fuel and products or air and products, which has been verified experimentally[7,8], so T_{RZ} and f_{RZ} do not vary in space.

To use the fundamental flame stability criterion (Eq. 12) it is necessary to determine the gas velocity U_s and the temperature T_s just upstream of the flame base. For a jet flame[35-37] the profiles of mean values of U/U_F and mixture fraction f should be equal everywhere because of the similarity between the conservation equations for these two quantities. Along the stoichiometric contour $U=U_s$ and $f=f_s$, so:

$$U_s = U_F f_s \Gamma \qquad (16)$$

Γ is a factor that accounts for gas expansion due to the flame, which causes streamlines to diverge[35-37]. An adequate explanation of measured liftoff heights is obtained by setting Γ equal to $c_1 (\delta/x)$, where c_1 is a constant and δ is the flame thickness α/S_L. When this value of Γ

is inserted into Eq. 16 and the value of x is set equal to h, one obtains the well-known relation for the liftoff height of a jet flame (Ref. 38):

$$h = c_1 U_F f_s / (S_0^2/\alpha_0) \qquad (17)$$

The blowout limit of a jet flame is determined by the criterion[30, 39] that the liftoff height cannot exceed the length of the flammable zone of the jet, which is (c_2 d), where d is the jet diameter and c_2 is a constant. Equating this length to the liftoff height given by Eq. 15, yields a blowout velocity of:

$$U_F = d (S_0^2/\alpha_0) (c_2/c_1) / f_s \qquad (18)$$

which has been verified by experiment[39]. Now consider the stratified shear layer shown in Fig. 3. We solve Eq. 15 for U and set $U=U_s$ after setting $f = f_s$ to obtain:

$$U_s = U_A (1 - f_s/f_{RZ}) \Gamma \qquad (19)$$

where Γ is a factor that accounts for gas expansion caused by a flame. For simplicity, we assume that Γ has the same value as for a jet flame ($c_1\delta/x$) and δ is α/S_{base}. Combining Eqs. 19 and 12 and setting x = h leads to:

$$S_{base} = U_A (1 - f_s/f_{RZ}) (c_1 \alpha/S_{base}) / h \qquad (20)$$

After applying our blowout criterion that $h = L_{RZ}$ (Eq. 14), rearrangement yields a relation for the required step height H to stabilize the flame:

$$(H/U_A) / (\alpha_0/S_0^2) = (L_{RZ}/H)^{-1} [S_{base}/S_0)]^{-2} [\alpha/\alpha_0] (1 - f_s/f_{RZ}) c_1 \qquad (21)$$

$(L_{RZ}/H)^{-1}$ is a constant for a particular geometry and S_0 and α_0 are the reference values of the stoichiometric laminar burning velocity and thermal diffusivity at 300 K and 1 atm. For hydrogen, ethylene, methane, and propane flames burning in air, it has been found [40-42] that :

$$S_{base}/S_0 = (T_s / 300K)^{1.75} (p /1 \text{ atm})^{-0.2} \qquad (22)$$

$$\alpha/\alpha_0 = (T_s / 300K)^{1.5} (p /1 \text{ atm})^{-1} \qquad (23)$$

The exponents in Eq. 22 represent an average of values reported in Refs. 40-42. Inserting Eqs. 22 and 23 into Eq. 21 leads to:

$$\left(\frac{H}{U_A} / \frac{\alpha_0}{S_0^2}\right) = \left[\frac{T_S}{300\,K}\right]^{-2} \left(\frac{p}{1\,atm}\right)^{-0.8} \left(1 - \frac{f_s}{f_{RZ}}\right) \left(\frac{L_{RZ}}{H}\right)^{-1} c_1$$

To determine the temperature (T_s) just upstream of the flame base which appears in Eq. 24, we solve Eq. 15 for T_0 and set $f = f_s$ and $T_0 = T_s$, assuming that at the stoichiometric contour the stagnation and static temperatures are nearly equal. This leads to:

$$T_s = T_{0A} + (f_s/f_{RZ}) (T_{RZ} - T_{0A}) \qquad (25)$$

The temperature in the recirculation zone (T_{RZ}) depends on the mass fraction of products $Y_{P,RZ}$, which coexist with fuel near the rich limit. Conservation of energy requires that:

$$T_{RZ} = Y_{P,RZ} T_{AD} + (1 - Y_{P,RZ}) T_F \qquad (26)$$

Combining Eqs. 25 and 26 yields:

$$T_s = T_{0A} + (f_s/f_{RZ}) [Y_{P,RZ} (T_{AD} - T_F) + (T_F - T_{0A})]$$

The problem has been reduced to that of determining the mass fraction of products in the recirculation zone ($Y_{P,RZ}$). The adiabatic flame temperature (T_{AD}) and initial fuel and air temperatures (T_F, T_{0A}) in Eq. 27 are given.

Parameters That Characterize Entrainment

The analysis leading to Eq. 27 indicates that an important parameter is the mass fraction of the product that are entrained into the recirculation zone ($Y_{P,RZ}$), since $Y_{P,RZ}$ governs the temperature of the recirculation zone. While it is not possible to calculate entrainment rates directly, the measurements reported in Refs. 4, 6, 33 and 43 yield some scaling relations that are proportional to the entrainment mass flowrates. Further research is needed to accurately determine the constants of proportionality, but only the general scaling relations are needed for the present work. First consider the shear layer in Fig. 7 that has a height δ_A at the downsteam end of the wall cavity shown. The mass flowrate of air that is entrained into a supersonic shear layer ($m_{A,SH}$) has been reported by Slessor and Dimotakis[43] to be:

$$m_{A,SH} = \rho_A U_A \delta_A W \qquad (28)$$

$$\delta_A = (0.17\,x) \frac{(1-r)(1+s^{1/2})}{(1+s^{1/2}r)} \left\{1 - \frac{(1-s^{1/2})/(1+s^{1/2})}{1+2.9\,(1+r)/(1-r)}\right\} \left[1 + 4\Pi_c^2\right]^{-1/2}$$

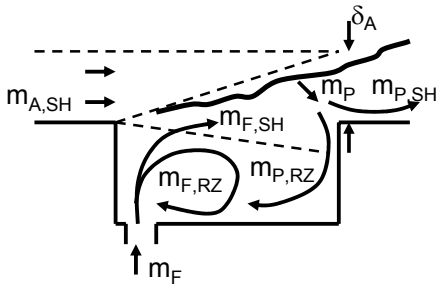

Figure 8. Schematic of the Entrainment of Fuel and Products into the Cavity Near the Rich Blowout Limit.

For the shear layer shown in Fig. 8, the density ratio (s) is approximately zero and the velocity ratio (r) also is approximately zero, since on the lower side of the shear layer the recirculation zone gases have relatively low density and low velocity. The convective Mach number term 4 Π_c^2 can be shown to be significantly less than one for the conditions considered herein, using the definition of Π_c that appears in Ref. 43. Inserting these values into Eqs. 28 and 29, and setting x equal to L_{RZ} yields:

$$m_{A,SH} = 0.13\ \rho_A\ U_A\ W\ L_{RZ} \qquad (30)$$

Near the rich blowout limit there is excessive fuel present, so Fig. 8 shows that the total fuel flowrate (m_F) is the sum of the fuel flowrate that enters the shear layer ($m_{F,SH}$) and the fuel flowrate that enters the recirculation zone ($m_{F,RZ}$). Similarly, the total mass flowrate of products produced (m_P) is the sum of that which enters the recirculation zone ($m_{P,RZ}$) and that which remains in the shear layer ($m_{P,SH}$). In the recirculation zone the fuel and products mix, so conservation of product mass requires that:

$$Y_{P,RZ} = m_{P,RZ} / (m_{P,RZ} + m_{F,RZ}) \qquad (31)$$

We now define two entrainment parameters:

$$\varepsilon_1 = m_{P,RZ} / m_P \qquad \varepsilon_2 = m_{F,RZ} / m_F \qquad (32)$$

so that Eq. 31 becomes:

$$Y_{P,RZ} = [1 + (\varepsilon_2/\varepsilon_1)\ (m_F / m_P)\ ]^{-1} \qquad (33)$$

Some justification for using the entrainment parameters defined by Eq. 32 was provided by Winterfeld[6]. He showed that the mass flowrate that is entrained from a supersonic stream into a recirculation zone is proportional to the mass flowrate that is entrained into the shear layer. He measured the entrained flowrate by continuously filling a cavity with boron fluoride which was suddenly discontinued; the rate at which the boron fluoride signal decayed in time indicated the rate at which dilution air was entrained into the cavity.

Conservation of mass requires that m_P equal the sum of the fuel and air mass flowrate into the shear layer ($m_{F,SH} + m_{A,SH}$). The stoichiometric fuel-air ratio (r_s) is ($m_{F,SH} / m_{A,SH}$) so it follows that:

$$m_P = m_{A,SH}\ (1 + r_s) \qquad (34)$$

The characteristic air mass flowrate (m_A) was defined by Eq. 3 to be $0.01\ \rho_A\ U_A\ H\ W$ so Eq. 30 becomes:

$$m_{A,SH} = m_A\ (0.04/0.01)\ (L_{RZ}/H)\ M_A^{-1} \qquad (35)$$

The result of inserting Eqs. 34 and 35 into Eq. 33 is:

$$Y_{P,RZ} = [\ 1 + \beta_1\ (L_{RZ}/H)^{-1}\ (m_F/m_A)]^{-1} \qquad (36)$$

β_1 is $(\varepsilon_2 / \varepsilon_1)\ (0.01/0.04)\ M_A\ (1 + r_s)^{-1}$. Note that Eq. 36 displays the correct physical trends. As the mass flowrate of fuel (m_F) is increased near the rich limit, more cold fuel mixes with hot products in the RZ; Eq. 36 indicates that the mass fraction of hot products decreases. This leads to a cooler recirculation zone, and less heating of the reactants ahead of the flame, leading to blowout.

One other quantity in Eq. 24 that must be estimated is the mixture fraction f_{RZ} at the lower edge of the shear layer. The standard assumption that is employed is that there exists a linear equilibrium state relation between mixture fraction and gas temperature for fuel-rich conditions, which is:

$$f = 1 - (1-f_s)\ (T - T_F) / (T_{AD} - T_F) \qquad (37)$$

Eq. 37 correctly indicates that for pure fuel ($T = T_F$) f is 1, and when $T = T_{AD}$, f equals f_s. We set $f = f_{RZ}$ and $T = T_{RZ}$, then replace T_{RZ} with the right side of Eq. 26 to yield:

$$f_{RZ} = 1 - (1- f_s)\ Y_{P,RZ} \qquad (38)$$

In Eq. 38 one can make the approximation that $f_s << 1$ so f_{RZ} becomes $(1–Y_{P,RZ})$.

Our final result for the rich limit is obtained by combining Eqs. 4, 24, 27, 36 and 38 to yield a relation that is identical to Eq. 6:

$$\left(\frac{H}{U} / \frac{a_0}{S_0^2}\right)_{RICH} \quad G_{RICH}^{-1} \quad = \quad \phi_O \qquad (39)$$

$$G_{RICH} = \left[\left[B \frac{(T_{AD} - T_F)}{300\ K} + \frac{(T_F - T_{0A})}{300\ K}\right] C + \frac{T_{0A}}{300\ K}\right]^{-2} \left(\frac{p}{1\ atm}\right)^{-0.8} D$$

B, C and D are defined by Eqs. 10 and 11. Eqs. 39 and 40 indicate that as the fuel mass flowrate (and ϕ_O) increase toward the rich limit, the cold fuel replaces products in the recirculation zone, so the mass fraction of hot products ($Y_{P,RZ}$) is reduced and the required step height H given by Eq. 39 increases. However, if the air stagnation temperature, fuel temperature or adiabatic flame temperature is increased, this reduces the required step height that is calculated using Eq. 37. Replacing hydrocarbon fuel with hydrogen increases S_0, so a smaller step is needed. All of the trends calculated using Eq. 39 are in agreement with the measurements described in the previous section. The analysis also agrees with the experimental observation[9] that increasing the fuel flowrate forces the flame liftoff position to move downstream until it exceeds L_{RZ} and blowout occurs.

Conclusions

1. Previously-measured step heights that are required to stabilize nonpremixed flames for 140 conditions were correlated using a Damkohler number and a scaling parameter (G) that are suggested by our analysis. Conditions in eleven previous studies covered the supersonic and subsonic regimes; geometries included cavities, bluff-bodies, and struts, and the fuels were hydrogen, ethylene, methane and propane. Previously such a correlation was reported only for subsonic, premixed flames.

2. Nonpremixed flame results differ significantly from the premixed case because the location of fuel injection is important, and the proper overall equivalence ratio must be defined. Fuel injection upstream of the recirculation zone enhances the lean limit but reduces the lean limit, while fuel injection directly into the recirculation zone has the opposite effect.

3. The analysis that leads to the scaling parameter G is consistent with several experimental observations: (a) fuel and air do not coexist and react in the recirculation zone, but hot products coexist with fuel near the rich limit and products and air coexist near the lean limit; (b) reactions occur in the shear layer, not the recirculation zone; (c) blowout is governed by the imbalance between the flame propagation speed and the gas velocity that occurs near the stoichiometric contour.

4. The analysis avoids the assumption that has been used in previous work, which requires the residence time of a mixture of fuel and air in the recirculation zone be matched to a chemical reaction time. Recent experiments show that this assumption is not valid since fuel and air do not coexist in the recirculation zone.

5. The relations derived in the analysis, which have been empirically validated, show how much the flame stability limits can be enhanced by increasing the step height, fuel injection temperature, and air 6. free stream stagnation temperature. The value of the stoichiometric fuel-air ratio (f_s) is important because it determines the distance between the stoichiometric contour and the airstream.

7. The poorest correlation occurred when fuels that have large differences in burning velocity, such as hydrogen and methane, are compared. This suggests that the square of the burning velocity, which appears in the Damkohler number, only partially explains the differences in blowout limits caused by changing the fuel type. The work identifies the need for additional measurements of entrainment rates from supersonic streams into recirculation zones, as well as the temperatures and mass fractions of species in the recirculation zone.

Acknowledgement

This work was supported by funds from NASA and the U.S. Air Force for the URETI Reusable Launch Vehicle Center located at the University of Maryland and the University of Michigan. The authors benefited from previous collaboration with researchers at the U.S.A.F. Wright Laboratories (Drs. J.M. Donbar, C.D. Carter, K.-Y. Hsu, M. R. Gruber).

References

1. Zukoski, E.E., and Marble, F.E., "Experiments Concerning the Mechanism of Flame Blowoff from Bluff-Bodies", Proceedings of the Gas Dynamics Symposium on

Thermochemistry, Northwestern U., Evanston, IL, p. 205, 1956.
2. Ozawa, R.I., "Survey of Basic Data on Flame Stabilization and Propagation for High Speed Combustion Systems", U.S. Air Force AFAPL Technical Report TR-70-81, 1970.
3. Plee, S.L. and Mellor, A.M., "Characteristic Time Correlation for Lean Blowoff of Bluff-Body Stabilized Flames", *Combustion and Flame* 35, 61-80, 1979.
4. Kundu, K., Banerjee, D., and Bhaduri, D., "Theoretical Analysis on Flame Stabilization by a Bluff-Body", *Combustion Science and Technology* 17, 153-162, 1977.
5. Baxter, M.R. and Lefebvre, A.H., "Flame Stabilization in High-Velocity Heterogeneious Fuel-Air Mixtures", *Journal of Propulsion and Power* 8,6, 1138-1143, 1992.
6. Winterfeld, G. "On the Process of Turbulent Exchange Behind Flame Holders", *Proceedings of the Combustion Institute* 10, 1265-1275, 1965.
7. Winterfeld, G. "Investigations on the Stabilization of Hydrogen Diffusion Flames in Supersonic Flow", DFVLR (Deutschen Forshungs-und Versuchsanstalt fur Luft und Raumfahrt) Report FB-76-35, 1976.
8. Gruber, M. R., Baurle, R.A., Mathur, T. and Hsu, K.-Y., "Fundamental Studies of Cavity-Based Flameholder Concepts for Supersonic Combustors", *Journal of Propulsion and Power* 17, 1, 146-153, 2001.
9. Rasmussen, C.C., Driscoll, J.F., Hsu, K.-Y., Donbar, J.M., Gruber, M., and Carter, C. "Stability Limits of Cavity-Stabilized Flames in Supersonic Flows", submitted to *Proceedings of the Combustion Institute* 30, 2004.
10. Gruber, M.R., Donbar, J.M., Carter, C.D., and Hsu, K.-Y., "Mixing and Combustion Studies Using Cavity-Based Flameholders in a Supersonic Flow", Sixteenth International Symposium on Air Breathing Engines, Cleveland, 2003; to appear, *Journal of Propulsion and Power*, 2004.
11. Ben-Yakar, A. and Hanson, R.K., "Cavity Flame-Holders for Ignition and Flame Stabilization in Scramjets: an Overview", *Journal of Propulsion and Power* 17, 4, 869-877, 2001.
12. Takahashi, S., Sato, N., Tsue, M., Kono, M., Nakamura, M., Kondo, H., and Ujiie, Y., "Control of Flameholding in Supersonic Airflow by Secondary Air Injection", *Journal of Propulsion and Power* 14,1, 18-23, 1998.
13. Niioka, T., Terada, K., Kobayashi, H., Hasegawa, S., "Flame Stabilization Characteristics of a Strut Divided into Two Parts in Supersonic Airflow", *Journal of Propulsion and Power* 11,1, 112-115, 1995.
14. Northam, G.B., Trexler, C.A., and McClinton, C., "Flame-holding Characteristics of a Swept Strut Hydrogen Fuel Injector for Scramjet Application", NASA TR A81-10711, 1981.
15. Yoon, Y., Donbar, J.M., and Driscoll, J.F., "Blowout Stability Limits of a Hydrogen Jet Flame in a Supersonic, Heated Coflowing Air Stream", *Combustion Science and Technology* 97, 137-156, 1994.
16. Huh, H., and Driscoll, J.F., "Shock-Wave Enhancement of the Mixing and Stability Limits of Supersonic Hydrogen-Air Jet Flames", *Proceedings of the Combustion Institute* 26, 2933-2939, 1996.
17. Schefer, R.W., Namazian, M., Kelly,J., and Perrin, M., "Effect of Confinement on Bluff-Body Burner Recirculation Zone Characteristics and Flame Stability", *Combustion Science and Technology* 120, 185-211, 1996.
18. Chen, Y.-C., Chang, C.-C., Pan, K.-L., and Yang, J.-T., "Flame Liftoff and Stabilization Mechanism of Nonpremixed Jet Flames on a Bluff-Body Burner", *Combustion and Flame* 115, 51-65, 1998.
19. Masri, A.R., and Bilger, R.W., "Turbulent Diffusion Flames of Hydrocarbon Fuels Stabilized on a Bluff Body", *Proceedings of the Combustion Institute* 20, 319-326, 1984.
20. Esquiva-Dano, I, Nguyen, H.T., and Escudie, D., "Influence of a Bluff Body's Shape on the Stabilization Regime of Nom-Premixed Flames", *Combustion and Flame* 127, 2167-2180, 2001.
21. Hsu, K.-Y., Goss, L.P., and Roquemore, W.M., "Characteristics of a Trapped-Vortex Combustor", *Journal of Propulsion and Power* 14,1, 57-65, 1998.
22. Katta, V. R., and Roquemore, W.M., "Study on Trapped Vortex Combustor- Effect of Injection on Flow Dynamics", *Journal of Propulsion and Power* 14,3, 273-281, 1998.
23. Feikema, D., Chen, R.-H., and Driscoll, J.F., "Enhancement of Flame Blowout Limits by the Use of Swirl", *Combustion and Flame* 80, 183-195.
24. Feikema, D, Chen, R.-H., and Driscoll, J.F., "Blowout of Nonpremixed Flames: Maximum Coaxial Air Velocities Achievable, with and without Swirl", *Combustion and Flame* 86, 347-358, 1991.
25. Rawe, R., and Kremer, H., "Stability Limits of Natural Gas Diffusion Flames with Swirl",

Proceedings of the Combustion Institute 18, 667-677, 1981.
26. Donbar, J.M., Driscoll, J.F., and Carter, C.D., "Reaction Zone Structure in Turbulent Nonpremixed Jet Flames – From CH-OH PLIF Images*, Combustion and Flame* 122, 1-19, 2000.
27. Namazian, M., Kelly, J.T., and Schefer, R.W., "Near Field Instantaneous Flame and Fuel Concentration Structures", *Proceedings of the Combustion Institute* 22, 627-634, 1988.
28. Schefer, R.W., Namazian, M. and Kelly, J., "CH, OH, and CH4 Concentration Measurements in a Lifted Turbulent Jet Flame*", Proceedings of the Combustion Institute* 23, 669-676, 1990.
29. Schefer, R.W., Namazian, M., and Kelly, J., "Stabilization of Lifted Turbulent-Jet Flames", *Combustion and Flame* 99, 75-86, 1994.
30. Vanquickenborne, L, and van Tiggelen, A., Combustion and Flame 10, 59-72, 1966.
31. Upatnieks, A., Driscoll, J.F., and Ceccio, S.L., "Cinema PIV Time History of the Propagation Velocity of the Base of a Lifted Turbulent Jet Flame", *Proceedings of the Combustion Institute* 29, 1898-1903, 2002.
32. Muniz, L., and Mungal, M.G., "Instantaneous Flame-Stabilization Velocities in Lifted Jet Diffusion Flames", *Combustion and Flame* 111, 16-31, 1997.
33. Kalt, P.A, Al-Abdeli, Y.M., Masri, A.R., and Barlow, R.S., "Swirling Turbulent Non-Premixed Flames of Methane: Flow Field and Compositional Structure", *Proceedings of the Combustion Institute*, Vol. 29, 1913-1919, 2002.
34. Ratner, A., Driscoll, J.F., Donbar, J.M., Carter, C.D., and Mullin, J.A., "Reaction Zone Structure of Non-Premixed Turbulent Flames in the "Intensely Wrinkled" Regime", *Proceedings of the Combustion Institute* 28, 245-252, 2000.
35. Chen, Y.-C., and Bilger, R.W., "Stabilization mechanisms of lifted laminar flames in axisymmetric jet flows", Combustion and Flame 123, 23- 45, 2000.
36. Upatnieks, A., Driscoll, J.F.,Rasmussen, C.C., and Ceccio, S.L.," Liftoff of Turbulent Jet Flames – Assessment of Edge Flame and Other Concepts Using Cinema-PIV Diagnostics", submitted *to Combustion and Flame*, 2004.
37. Boulanger, J., Vervisch, Reveillon, Ghosal, S., "Effects of Heat Release in Laminar Diffusion Flames Lifted on Round Jets", *Combustion and Flame* 134, 355-368, 2003.
38. Kalghatgi, G. "Liftoff Heights and Visible Lengths of Vertical Turbulent Jet Diffusion flames in Still Air", *Combustion Science and Technology* 41, 17-29, 1984.
39. Kalghatgi, G. "Blow-Out Stability of Gaseous jet Diffusion Flames in Still Air", *Combustion Science and Technology* 26, 233-239, 1981.
40. Iijima, T., and Takeno, T., "Effects of Temperature and Pressure on Burning Velocity", *Combustion and Flame* 65, 35-43, 1986.
41. Muller, U.C., Bollig, M., and Peters, N., "Approximations for Burning Velocities and Markstein Numbers for Lean Hydrocarbons and Methanol Flames", *Combustion and Flame* 108, 349-356, 1997.
42. Gulder, O.L., "Laminar Burning Velocities of Methanol, Ethanol, and Isooctane-Air Mixtures", *Proceedings of the Combustion Institute* 19, 275-281, 1982.
43. Slessor, M.D., Zhuang, M., and Dimotakis, P.E., "Turbulent Shear-Layer Mixing: Growth-Rate Compressibility Scaling", Journal of Fluid Mechanics 414, 35-45, 2000.
44. Glassman, I. Combustion, 2nd Ed., pg. 254, Academic Press, New York, N.Y. 1987.